Separation Science and Technology
Publication details, including instructions for authors and subscription information:
http://www.informaworld.com/smpp/title~content=t713708471

Soil Clean Up by in-situ Aeration. VI. Effects of Variable Permeabilities

Cesar Gomez-lahoz[a]; Jose M. Rodriguez-maroto[a]; David J. Wilson[b]
[a] DEPARTAMENTO DE INGENIERIA, QUIMICA UNIVERSIDAD DE MALAGA, MALAGA, SPAIN [b] DEPARTMENTS OF CHEMISTRY AND OF ENVIRONMENTAL AND CIVIL ENGINEERING, VANDERBILT UNIVERSITY NASHVILLE, TENNESSEE

To cite this Article Gomez-lahoz, Cesar , Rodriguez-maroto, Jose M. and Wilson, David J.(1991) 'Soil Clean Up by in-situ Aeration. VI. Effects of Variable Permeabilities', Separation Science and Technology, 26: 2, 133 — 163
To link to this Article: DOI: 10.1080/01496399108050463
URL: http://dx.doi.org/10.1080/01496399108050463

SEPARATION SCIENCE AND TECHNOLOGY, 26(2), pp. 133–163, 1991

Soil Clean Up by *in-situ* Aeration. VI. Effects of Variable Permeabilities

CESAR GOMEZ-LAHOZ and JOSE M. RODRIGUEZ-MAROTO
DEPARTAMENTO DE INGENIERIA QUIMICA
UNIVERSIDAD DE MALAGA
29071 MALAGA, SPAIN

DAVID J. WILSON*
DEPARTMENTS OF CHEMISTRY AND OF ENVIRONMENTAL AND CIVIL ENGINEERING
VANDERBILT UNIVERSITY
NASHVILLE, TENNESSEE 37235

Abstract

A mathematical model for *in-situ* soil vapor stripping (vacuum extraction) is developed and used to examine the effects of a spatially variable pneumatic permeability tensor on the rate of clean-up of a site contaminated with volatile organic compounds. Runs are made with low-permeability clay lenses placed at various locations in the domain of interest; also the effect of soil moisture distribution on the soil gas flow field is examined. The model permits one to carry out a sensitivity analysis of the effects of heterogeneity in the permeability, and to develop strategies for minimizing the damaging effects of domains of low permeability.

INTRODUCTION

Soil vapor stripping (vacuum extraction) has become an important tool in the remediation of hazardous waste sites contaminated with volatile organic compounds (VOCs) in the vadose zone. Osejo and Wilson (*1*) reviewed much of the recent literature on the subject in a paper on mathematically modeling the vapor stripping of nonaqueous phase liquid (NAPL) floating on the water table under the vadose zone. Earlier papers in this series dealt with the development of a model based on Henry's law and the local equilibrium assumption, the effects of well geometrical pa-

*To whom correspondence should be addressed.

rameters, the effects of overlying impermeable caps and passive wells, the effects of strata of differing permeabilities and of anisotropic permeabilities, and the effects of diffusion-limited mass transport in the vapor stripping of fractured bedrock (*2–6*). Other work on the modeling of soil vapor stripping of particular relevance to the present study includes the investigations of Hoag and his associates on the vapor stripping of gasoline (*7, 8*), and the work of Hutzler, McKenzie, and Gierke (*9*). Hoag's model assumes local equilibrium; the one-dimensional model of Hutzler et al. takes into account diffusion and air–water mass transfer rate.

By and large, present models for soil vapor stripping assume that the pneumatic permeability of the soil in the domain of interest is constant and isotropic. One of our earlier papers (*5*) dealt with stratified soils and with constant anisotropic permeabilities, and it was remarked that the presence of horizontal strata and/or an anisotropic permeability resulted in rather substantial changes in the soil gas pressures and flow patterns around a vacuum well. Jury (*10*) has noted that there is a great deal of vertical and lateral variability in virtually all the parameters characterizing soil transport processes. Permeability measurements typically show a log normal distribution (*11*), and sets of permeability data typically yield correlation lengths which depend strongly on the scale of the measurements. Examination of well logs at most hazardous waste sites quickly yields qualitative information indicating that the soil is quite heterogeneous.

We were therefore interested in assessing the extent to which the expected variations in the pneumatic permeability tensor would affect the results of vapor stripping model calculations. We very much hope that no one regards vapor stripping model calculations as a high-precision activity; still, one would like to feel that one could rely on calculated times required for remediation to, say, ±30%. A highly variable pneumatic permeability might well introduce variations in calculated clean-up times substantially larger than this, we feared. Also, if one has information about the locations of the zones of low permeability, perhaps one could design the array of vapor stripping wells so as to reduce their interference with the clean-up. Here we explore the effects of lens-shaped domains of low permeability on the shapes of the streamlines of the soil gas in the vicinity of a vapor stripping horizontal lateral slotted pipe and on the rate of clean-up of the soil in the domain of influence of this pipe. We also examine the effects of spatial variation in the soil moisture content.

ANALYSIS

Our previous field vapor stripping well models have been axially symmetric, describing a single vertical well. An alternative geometry is that in

which parallel horizontal slotted laterals are placed in the soil; this approach was used for decontaminating soil at Hill Air Force Base, Utah (*12*, *13*). This allows us to use two Cartesian space coordinates, and thereby to construct a model which can easily run on currently available microcomputers.

We first address the calculation of the soil gas velocity field in the vicinity of the well. See Fig. 1 for notation. The surface of the soil is a distance l_y above the water table, and the spacing between adjacent laterals is l_x. The soil gas pressure $P(x,y)$ satisfies the equation

$$\nabla \cdot \mathbf{K} \nabla P^2 = 0 \tag{1}$$

where

$$\mathbf{K} = \begin{pmatrix} K_x(x,y) & 0 \\ 0 & K_y(x,y) \end{pmatrix}$$

is the pneumatic permeability tensor.

The boundary conditions are

$$P^2(x,l_y) = P_a^2 = 1 \text{ atm}^2 \tag{2}$$

$$\frac{\partial P^2(0,y)}{\partial x} = 0 \tag{3}$$

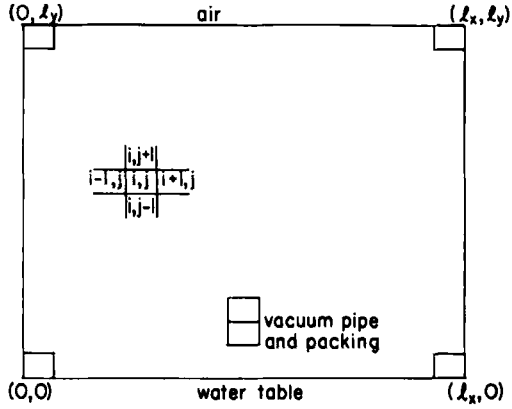

FIG. 1. Geometry and notation, vapor stripping with long horizontal slotted lateral pipes.

$$\frac{\partial P^2(lx,y)}{\partial x} = 0 \tag{4}$$

$$\frac{\partial P^2(x,0)}{\partial y} = 0 \tag{5}$$

Equations (3) and (4) represent the stagnation planes located roughly half way between two adjacent laterals, or they may represent impermeable cut-off walls. Equation (5) represents the no-flow condition imposed by the water table. In addition, we require a sink at $(l_x/2,h)$ to represent the effect of the lateral vacuum pipe.

Since K_x and K_y may be rather complicated functions of x and y, we employ a numerical method, over relaxation (*14*), to obtain $P^2(x,y)$. The soil gas velocity values are then calculated from

$$v = -K\nabla P \tag{6}$$

by means of finite differences.

We define a mesh over the space of interest as follows:

$$x_i = (i + 1/2)\Delta x, \qquad i = 0, 1, 2, \ldots, n_x$$

$$y_j = (j + 1/2)\Delta y, \qquad j = 0, 1, 2, \ldots, n_y$$

where

$$n_x = (l_x/\Delta x) - 1$$

$$n_y = (l_y/\Delta y) - 1$$

$$P^2_{ij} = P^2(x_i,y_j)$$

Then the finite difference approximation to Eq. (1) is

$$\begin{aligned} 0 = {} & K_x(i\Delta x\cdot(j + 1/2)\Delta y)(P^2_{i-1,j} - P^2_{i,j})(\Delta y/\Delta x) \\ & + K_x((i + 1)\Delta x\cdot(j + 1/2)\Delta y)(P^2_{i+1,j} - P^2_{i,j})(\Delta y/\Delta x) \\ & + K_y((i + 1/2)\Delta x\cdot(j\Delta y)(P^2_{i,j-1} - P^2_{i,j})(\Delta x/\Delta y) \\ & + K_y((i + 1/2)\Delta x\cdot(j + 1)\Delta y)(P^2_{i,j+1} - P^2_{i,j})(\Delta x/\Delta y) \end{aligned} \tag{7}$$

for a general interior point. This is solved for $P^2_{i,j}$, which yields

$$P^2_{i,j} = \frac{\begin{array}{c}[K_x(i,j+1/2)\delta P^2_{i-1,j} + K_x(i+1,j+1/2)\delta P^2_{i+1,j} \\ + K_y(i+1/2,j)\delta^{-1}P^2_{i,j-1} + K_y(i+1/2,j+1)\delta^{-1}P^2_{i,j+1}]\end{array}}{\begin{array}{c}[K_x(i,j+1/2)\delta + K_x(i+1,j+1/2)\delta \\ + K_y(i+1/2,j)\delta^{-1} + K_y(i+1/2,j+1)\delta^{-1}]\end{array}} \tag{8}$$

where $\delta = \Delta y/\Delta x$ and we have simplified the notation for K_x and K_y; $K_x(i,j) = K_x(i\Delta x, j\Delta y)$, etc.

The boundary condition represented by Eq. (3) transcribes into the finite difference representation as

$$P^2_{0j} = \frac{\begin{array}{c}[K_x(1,j+1/2)\delta P^2_{1,j} + K_y(1/2,j)\delta^{-1}P^2_{0,j-1} \\ + K_y(1/2,j+1)\delta^{-1}P^2_{0,j+1}]\end{array}}{[K_x(1,j+1/2)\delta + K_y(1/2,j)\delta^{-1} + K_y(1/2,j+1)\delta^{-1}]} \tag{9}$$

Equation (4) yields

$$P^2_{nx,j} = \frac{\begin{array}{c}[K_x(n_x,j+1/2)\delta P^2_{nx-1,j} + K_y(n_x+1/2,j)\delta^{-1}P^2_{nx,j-1} \\ + K_y(n_x+1/2,j+1)\delta^{-1}P^2_{nx,j+1}]\end{array}}{\begin{array}{c}[K_x(n_x,j+1/2)\delta + K_y(n_x+1/2,j)\delta^{-1} \\ + K_y(n_x+1/2,j+1)\delta^{-1}]\end{array}} \tag{10}$$

Equation (5) yields

$$P^2_{i,0} = \frac{\begin{array}{c}[K_x(i,1/2)\delta P^2_{i-1,0} + K_x(i+1,1/2)\delta P^2_{i+1,0} \\ + K_y(i+1/2,1)\delta^{-1}P^2_{i,1}]\end{array}}{[K_x(i,1/2)\delta + K_x(i+1,1/2)\delta + K_y(i+1/2,1)\delta^{-1}]} \tag{11}$$

The boundary condition at the top of the domain, Eq. (2), yields

$$P^2_{i,ny} = \frac{\begin{array}{c}[K_x(i,n_y+1/2)\delta P^2_{i-1,ny} + K_x(i+1,n_y+1/2)\delta P^2_{i+1,ny} \\ + K_y(i+1/2,n_y)\delta^{-1}P^2_{i,ny-1} + 2K_y(i+1/2,n_y+1)\delta^{-1}P^2_a]\end{array}}{\begin{array}{c}[K_x(i,n_y+1/2)\delta + K_x(i+1,n_y+1/2)\delta \\ + K_y(i+1/2,n_y)\delta^{-1} + 2K_y(i+1/2,n_y+1)\delta^{-1}]\end{array}} \tag{12}$$

Similar expressions are obtained for the corner volume elements.

The mean pressure within the volume element containing the lateral pipe is estimated as follows. The pressure in the vicinity of the pipe is given

approximately by

$$P^2(r) = P_w^2 + \frac{P_a^2 - P_w^2}{\log (l/a)} \log (r/a) \tag{13}$$

where P_a = ambient atmospheric pressure, atm
P_w = wellhead pressure, atm
a = pipe radius (or radius of gravel packing, if present), m
l = a length of the order of the distance from the pipe to the surface of the soil, approximately l_y m

One approach is to calculate the mean value of P^2 in an annular domain about the pipe of inner radius a and outer radius b, where

$$b = \left(\frac{\Delta x \cdot \Delta y}{\pi}\right)^{1/2}$$

This is given by

$$\overline{P}^2 = \int_a^b P^2(r) r dr \Big/ \int_a^b r dr$$

which, on use of Eq. (13) and integration, yields

$$\overline{P}^2 = P_w^2 + (P_a^2 - P_w^2)\left(\frac{\log (b/a)}{1 - a^2/b^2} - 1/2\right)\frac{1}{\log (l/a)} \tag{14}$$

We may take this value for $P_{l,0}^2$, the value of the pressure in the domain $\Delta x \Delta y$ containing the lateral pipe; we set $l = l_y$.

An alternative method of obtaining the effective pressure in the domain containing the sink is developed as follows. Again we start with Eq. (13) as an approximate expression for the pressure in the vicinity of the slotted lateral pipe. The molar gas flow rate per unit length of pipe is then given by

$$Q = \frac{K v \Delta P^2 \cdot \pi r}{RT} \tag{15}$$

for any value of r.

From Eq. (13),

$$\nabla_r P^2 = \frac{P_a^2 - P_w^2}{\log (l/a)} \frac{1}{r}$$

Now we wish to have the flux $Q(a)$ from the actual lateral pipe of packed radius a equal to the flux $Q(\Delta x/2)$ from a lateral pipe of radius $\Delta x/2$ located in the same position in the domain of interest. We accomplish this by our choice of the pressure in the volume element containing the lateral pipe, $P_{l,0}$. This yields, after some cancellations,

$$\frac{P_a^2 - P_w^2}{\log (l/a)} = \frac{P_a^2 - P_{l,0}^2}{\log (2l/\Delta x)}$$

which rearranges to give

$$P_{l,0}^2 = P_a^2 - (P_a^2 - P_w^2) \frac{\log (2l/\Delta x)}{\log (l/a)} \tag{16}$$

Equations (7)–(12) (and the corresponding equations for the volume elements at the corners of the domain of interest) are then solved by overrelaxation for the $P_{i,j}^2$; $P_{l,0}^2$ is held equal to the value of $P_{l,0}^2$ obtained from Eqs. (14) or (16). The algorithm is as follows.

$$P_{ij}^{2*} = f(\{P_{kl}^2\}) \tag{17}$$

is the relaxation step. Then

$$P_{ij}^{2\#} = \omega P_{ij}^{2*} + (1 - \omega) P_{ij}^2, \qquad 1 < \omega < 2 \tag{18}$$

calculates the over relaxed values of the P_{ij}^2, which are then used in the next iteration. Actually, the newly computed values $P_{ij}^{2\#}$ are immediately put back into the array for the P_{ij}^2; this speeds convergence somewhat and reduces memory requirements. Convergence of these calculations requires of the order of a minute for a 10 × 20 array on an MMG 286 microcomputer operating at 20 MHz. A value of 1.8 was generally used for ω.

Soil gas streamlines and their transit times are very helpful in quickly identifying regions of the domain of interest which will clean up slowly. A fundamental truth in soil vapor stripping is that gas must be supplied to any domain which is to be cleaned up. The streamlines are calculated by

integration of the equations

$$\frac{dx}{dt} = -K_x(x,y)\frac{\partial P}{\partial x} \tag{19}$$

$$\frac{dy}{dt} = -K_y(x,y)\frac{\partial P}{\partial y} \tag{20}$$

For interior points (not in volume elements at the border of the domain) we calculate these derivatives from the Taylor's series for the pressure. In the ijth volume element

$$P(x,y) = P_{ij} + \frac{\partial P}{\partial x_{ij}}(x - x_i) + \frac{\partial P}{\partial y_{ij}}(y - y_j) + 1/2\frac{\partial^2 P}{\partial x_{ij}^2}(x - x_i)^2 + 1/2\frac{\partial^2 P}{\partial y_{ij}^2}(y - y_j)^2 + \frac{\partial^2 P}{\partial x \partial y_{ij}}(x - x_i)(y - y_j) \tag{21}$$

where

$$\partial P/\partial x_{ij} = (P_{i+1,j} - P_{i-1,j})/2\Delta x \tag{22}$$

$$\partial P/\partial y_{ij} = (P_{i,j+1} - P_{i,j-1})/2\Delta y \tag{23}$$

$$\partial^2 P/\partial x_{ij}^2 = (P_{i+1,j} - 2P_{i,j} + P_{i-1,j})/\Delta x^2 \tag{24}$$

$$\partial^2 P/\partial y_{ij}^2 = (P_{i,j+1} - 2P_{i,j} + P_{i,j-1})/\Delta y^2 \tag{25}$$

$$\partial^2 P/\partial x \partial y_{ij} = (P_{i+1,j+1} - P_{i-1,j+1} - P_{i+1,j-1} + P_{i-1,j-1})/4\Delta x \Delta y \tag{26}$$

These formulas can also be used on the left, right, and bottom borders by replacing $P_{-1,j}$ by $P_{0,j}$ along the left border, $P_{i,-1}$ by $P_{i,0}$ along the bottom border, and $P_{nx+1,j}$ by $P_{nx,j}$ along the right border, which causes the no-flow boundary conditions to be satisfied. At the top boundary, Taylor's series expansions yield

$$\partial P/\partial y_{i,ny} = -[1/3 \cdot P_{i,ny-1} + P_{i,ny} - 4/3 \cdot P_a]/\Delta y \tag{27}$$

$$\partial^2 P/\partial y_{i,ny}^2 = 4[P_{i,ny-1} - 3P_{i,ny} + 2P_a]/3\Delta y^2 \tag{28}$$

and

$$\frac{\partial^2 P}{\partial x \partial y_{i,ny}} = \frac{(1/3)(P_{i+1,ny-1} - P_{i-1,ny-1}) + (P_{i+1,ny} - P_{i-1,ny})}{2\Delta x \Delta y} \tag{29}$$

where P_a is the ambient atmospheric pressure. These formulas appear to be somewhat more accurate in the border regions than some we have used earlier; with these we get well-behaved streamlines right out to the edges of the domain. Transit times are calculated by simply keeping track of the accumulating value of t in the numerical integrations generating the streamlines.

The movement of volatile organic compounds (VOCs) under the influence of the flow field generated by the horizontal lateral vacuum pipe is assumed to be governed by the equation

$$\frac{\partial m}{\partial t} = -\frac{\nabla \cdot \mathbf{v}m}{v + w/K_H} \tag{30}$$

where m = mass of contaminant per unit volume of soil, kg/m^3
$\mathbf{v}$ = soil gas velocity, m/s
w = specific volumetric moisture content, dimensionless
v = voids fraction
K_H = effective Henry's constant of the VOC in the matrix of interest

The dispersion term is omitted from Eq. (30), to be represented by the effects of numerical dispersion. The equation is approximated by an array of ordinary differential equations defined at the mesh points of the domain, as above. Then

$$\frac{dm_{ij}}{dt} = \frac{1}{v + w/K_H}\left\{\frac{v_x(i,j+1/2)}{\Delta x}[S(v_x)m_{i-1,j} + S(-v_x)m_{ij}]\right.$$

$$- \frac{v_x(i+1,j+1/2)}{\Delta x}[S(v_x)m_{ij} + S(-v_x)m_{i+1,j}]$$

$$+ \frac{v_y(i+1/2,j)}{\Delta y}[S(v_y)m_{i,j-1} + S(-v_y)m_{ij}]$$

$$\left. - \frac{v_y(i+1/2,j+1)}{\Delta y}[S(v_y)m_{ij} + S(-v_y)m_{i,j+1}]\right\} \tag{31}$$

where

$$v_x(i,j + 1/2) = -K_x(i\Delta x,(j + 1/2)\Delta y)(P_{ij} - P_{i-1,j})/\Delta x$$

$$v_y(i + 1/2,j) = -K_y((i + 1/2)\Delta x,j\Delta y)(P_{ij} - P_{i,j-1})/\Delta y \quad (32)$$

etc., and

$$S(u) = 1, u > 0$$

$$= 0, u < 0$$

An initial contaminant distribution is established in the domain of interest, and then Eqs. (31) are integrated forward in time. The total mass of contaminant per meter of domain length (in the direction of the horizontal laterals) is given by

$$M_{\text{total}}(t) = \sum_i \sum_j m_{ij}(t)\Delta x\Delta y \quad (33)$$

Our objective here is to explore the effects of spatial variations in the permeability tensor. To do this we choose

$$K_x(x,y) = K_{x0} - \sum_{i=1}^{m} A_i \exp\left\{-\left[\left(\frac{x - x_i}{r_i}\right)^2 + \left(\frac{y - y_i}{s_i}\right)^2\right]^n\right\},$$

$$n = 1 \text{ or } 2 \quad (34)$$

with a similar expression for $K_y(x,y)$. This allows us to represent low-permeability "lenses" of thickness $2s_i$ and width $2r_i$. Such structures are not uncommon in soils.

RESULTS, LOW-PERMEABILITY LENSES

A set of eight runs was made to explore the effects of low permeability lenses on the soil gas streamlines and on the rate of clean up of the domain. The standard run parameters are given in Table 1. The parameters characterizing the lenses are given in the captions to the figures. The numbers by the streamlines are the transit times in 10^3 seconds for the soil gas to move from the surface of the ground to the lateral pipe well. For this set of runs, Eq. (16) was used to calculate $P^2_{I,0}$. Figure 2 shows the streamlines for Run 1, for which no lenses were present.

TABLE 1
Standard Parameter Set for the Runs shown in Figures 2–12

Domain length	13 m
Domain depth	8 m
dx, dy	1 m
Location of well	x = 6.5 m, y = 0.5 m
Packed radius of well	0.2 m
Wellhead pressure	0.85 atm
Temperature	14°C
Soil gas-filled porosity	0.3
K_{x0}, K_{y0}	0.100 m²/atm · s
Initial soil contaminant concentration	100 mg/kg
Soil density	1.7 g/mL
Specific moisture content	0.2
Effective Henry's constant	0.005

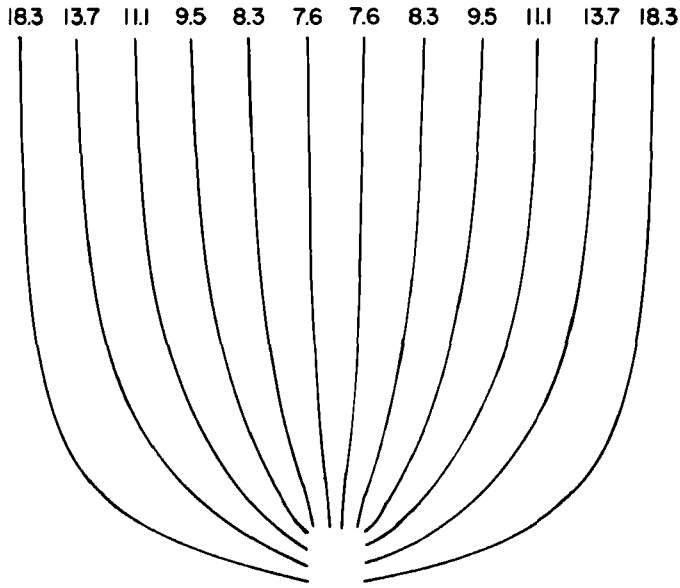

FIG. 2. Streamlines in the absence of low permeability lenses (Run 1). The numbers at the tops of the streamlines are the gas transit times in units of 1000 s. See Table 1 for model parameters for Runs 1–8.

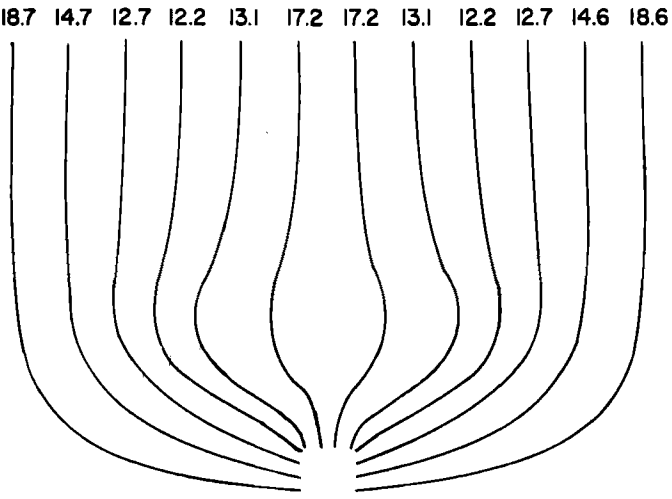

FIG. 3. Streamlines in the presence of a lens centered over the vapor extraction well. The lens is centered at the point (6.5, 3). $A_1 = B_1 = 0.095$ m²/atm · s, $r_1 = 3$ m, $s_1 = 1$ m, $n = 2$. Run 2.

In Fig. 3, Run 2, we see the distortion of the streamlines resulting from the presence of a lens centered over the vapor extraction well and a short distance above its screened section. The transit times are markedly different from those obtained in the absence of a lens (Fig. 2), but none are appreciably larger than the maximum time seen in Fig. 2. We therefore expect that the presence of a lens in this position will have relatively little effect on the overall rate of cleanup. As we shall see shortly, this is in fact the case.

Figure 4 (Run 3) shows streamlines for a run with a lens above and somewhat to the left of the vacuum well. Three of the streamlines have transit times which are somewhat larger than the maximum observed in Fig. 2. As one might therefore expect, this results in a somewhat slower rate of cleanup.

Run 4, in Fig. 5, is an excellent illustration of poor placement of a vacuum well relative to a low-permeability lens. The lens, far on the left side of the domain of influence, has very markedly reduced the flow of soil gas through the lower left portion of the domain, as indicated by both the long transit time of the leftmost streamline and the shapes of the streamlines. We therefore expect a substantial decrease in cleanup rate for this run.

Run 5, shown in Fig. 6, represents the ultimate disaster in the placement of a vapor-stripping well. The vapor-stripping well is screened right in the

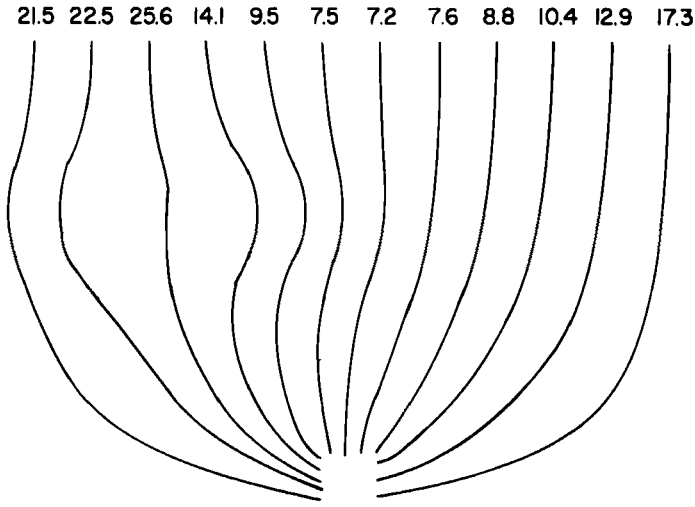

FIG. 4. Streamlines in the presence of a lens in the upper left portion of the domain, centered at (3, 5). Other lens parameters as in Fig. 3. Run 3.

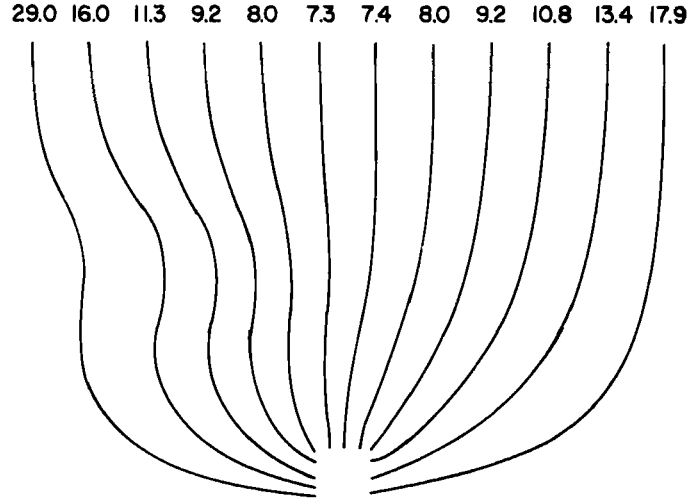

FIG. 5. Streamlines in the presence of a lens in the far left portion of the domain, centered at (1, 4). $r_1 = 4$, $s_1 = 1$ m, other parameters as in Fig. 3. Run 4.

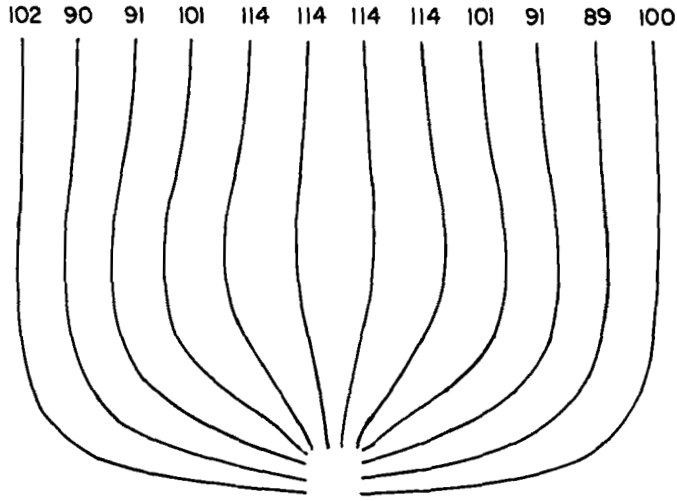

FIG. 6. Streamlines in the presence of a lens surrounding the screened section of the well, centered at (6.5, 2). $r_1 = s_1 = 4$ m, other parameters as in Fig. 3. Run 5.

middle of the low-permeability lens. This has reduced the molar flow rate from a value of 0.218 mol/s (no lens, Run 1) to 0.0265 mol/s, one-eighth of the reference flow rate. The transit times of the soil gas have been correspondingly increased, and we therefore expect a greatly reduced rate of cleanup.

Figure 7 shows plots of $\log_{10}$(total contaminant mass) versus time for Runs 1 through 5. We see that, as expected, the lens in Run 2 (Fig. 3) has

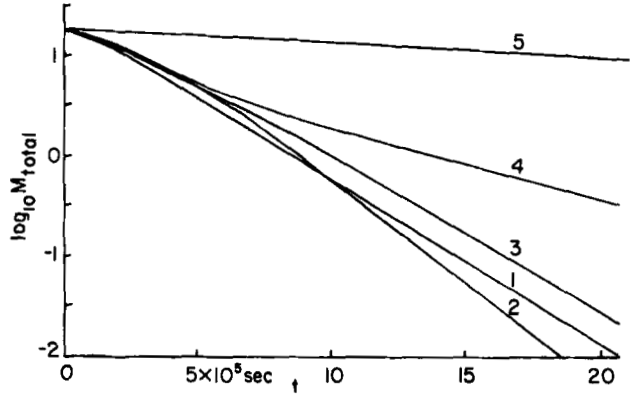

FIG. 7. Plots of $\log_{10}$ (total contaminant mass, M_{total}) versus time for Runs 1 through 4.

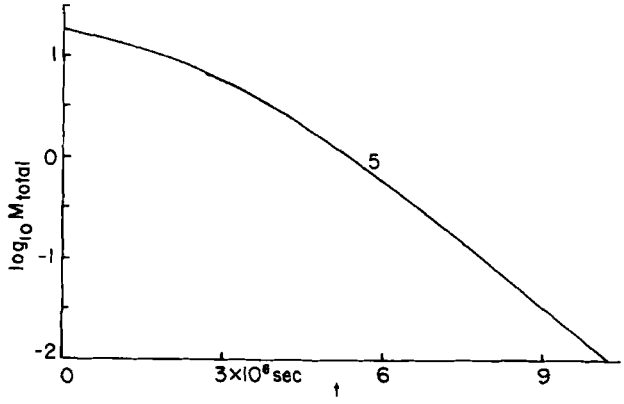

FIG. 8. Plot of $\log_{10}(M_{total})$ versus time for Run 5.

had little effect on the rate of cleanup of this system. The off-center lens in Run 3 (Fig. 4) has slowed down the rate of cleanup slightly. The lens, which was located far on the left side of the domain (Run 4, Fig. 5), has very markedly reduced the rate of cleanup; the slope of the plot for Run 1 is 2.25 times the slope of the plot for Run 4 in the linear sections of the

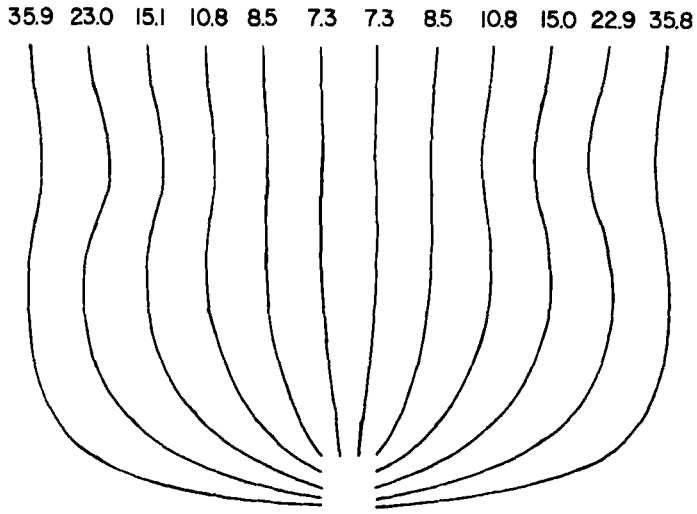

FIG. 9. Streamlines in the presence of low permeability lenses in the upper right and upper left corners of the domain, centered at (1, 6) and (12, 6). $r_i = 4$, $s_i = 1$ m, $A_i = B_i = 0.095$ m²/atm · s ($i = 1, 2$), $n = 1$. Run 6.

plots. The plot of $\log_{10}(M_{total})$ versus t for Run 5 (Fig. 8) shows that the effect of screening the well in the middle of the low-permeability lens was indeed disastrous, due principally to the decreased molar gas flow rate through the well in Run 5 as compared to Run 1. 99% cleanup from an initial contaminant mass of 17.68 kg required 15.9 days in Run 1; it required 85 days in Run 5, as seen in Fig. 8.

The inclusion of more than one low permeability lens is illustrated in Runs 6, 7, and 8 (Figs. 9, 10, 11, and 12). Here a lens is located on either side of the domain, focusing the soil gas flow toward the center plane of the domain. As seen in Fig. 12, the rates of cleanup in Runs 6, 7, and 8 are somewhat reduced below that found in the absence of any lenses. We note that in the model being used, the cleanup times are inversely proportional to the effective Henry's constant K_H.

Nine other runs were made with somewhat different model parameters in exploring the effects of lenses of decreased permeability. The model parameters describing the overall domain and the well characteristics are given in Table 2. The parameters describing the size, shape, and permeability of the lenses are given in Table 3. The positions of the centers of the lenses are shown in Fig. 13. Run 9, for which streamlines are shown in Fig. 20, pertains to a system having no low permeability lenses; its

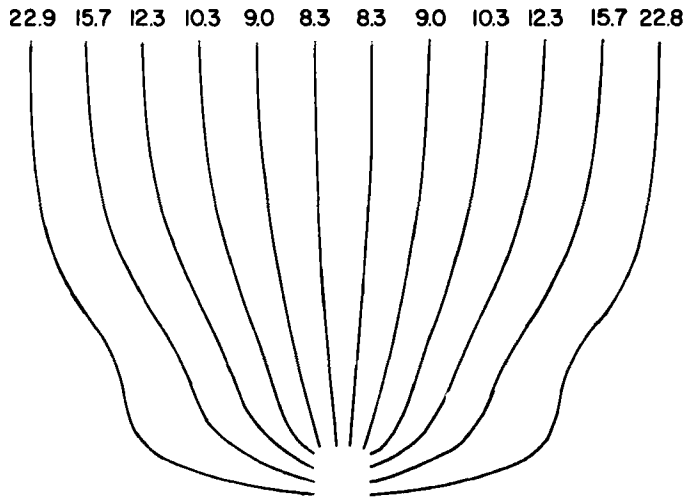

FIG. 10. Streamlines in the presence of low permeability lenses in the lower right and lower left corners of the domain, centered at (1, 2) and (12, 2). Other parameters as in Fig. 9. Run 7.

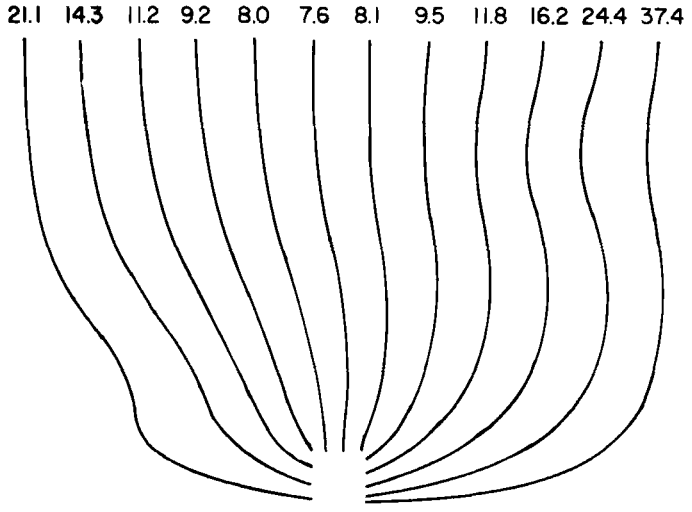

FIG. 11. Streamlines in the presence of low permeability lenses in the upper right and lower left corners of the domain, centered at (1, 2) and (12, 6). Other parameters as in Fig. 9. Run 8.

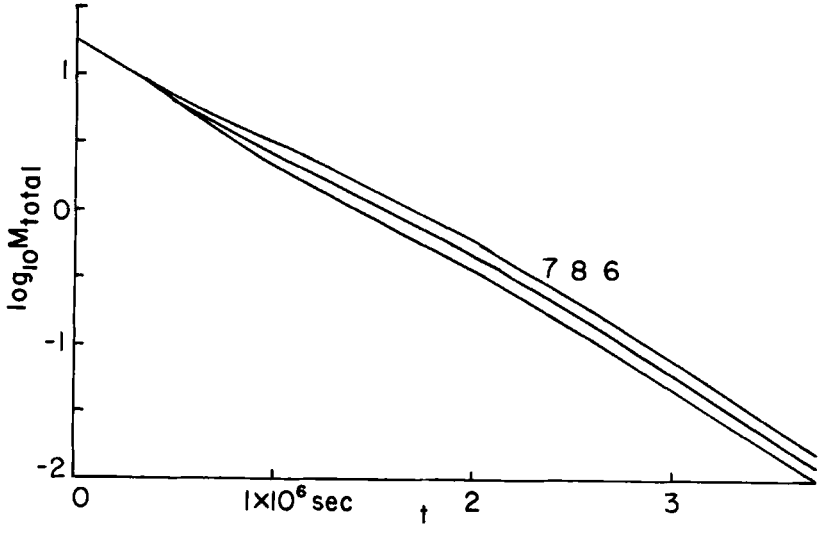

FIG. 12. Plots of $\log_{10}(M_{total})$ versus t for Runs 6, 7, and 8.

TABLE 2
Geometrical and Physical Parameters for the Model, Runs 9–17 and 18–38

Depth of domain	12 m
Width of domain	25 m
dx	1 m
dy	0.6 m
Wellhead pressure	0.75 atm
Height of bottom of screened well section above the water table	1.2 m
Height of top of screened well section above the water table	3.0 m
Effective Henry's constant	0.001
Initial total contaminant mass	10 kg
Permeabilities K_{x0} and K_{y0}	0.1 m^2/atm · s
Temperature	25°C

parameters are given in Table 2. In these runs, $P_{l,0}^2$ was obtained from Eq. (14).

Streamlines and transit times for Runs 10 and 14 are shown in Figs. 14 and 15. The placement of the horizontal vacuum extraction pipe a short distance above the water table does not make any substantial difference in the gas flow field as compared to the results obtained above with the vacuum pipe essentially at the water table.

Plots of $\log_{10}$ (total contaminant mass) versus time for nine of these runs are shown in Figs. 16 and 17. We see that the 99.9% cleanup times for three of the systems containing lenses are shorter than the time required for 99.9% cleanup in Run 9, in which no lens is present. In Run 10 the lens close to the surface causes a decrease in the very rapid rate of cleanup of the soil near the well, but also increases the rate of cleanup of the soil near the sides of the domain by deflecting gas flow into these regions. Since these regions are particularly slow to clean up, the net result is an increase in the overall rate of contaminant removal. In Run 14 (Fig. 15), observe that again the presence of the lens forces the flow of soil gas out

TABLE 3
Parameters Describing the Lenses, Runs 9–17

A_i	0.095 m^2/atm · s
B_i	0.095 m^2/atm · s
r_i	6.0 m
s_i	1.5 m
n	1

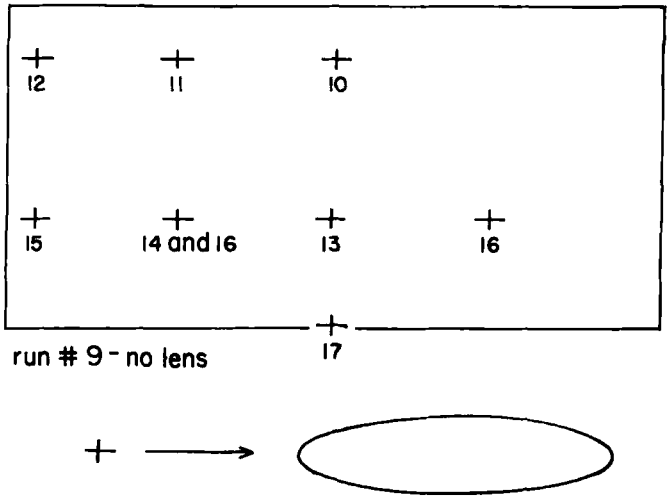

FIG. 13. Positions of the centers of the low permeability lenses for Runs 10–16. Run 9, the reference run, has no lenses. See Tables 2 and 3 for parameter values.

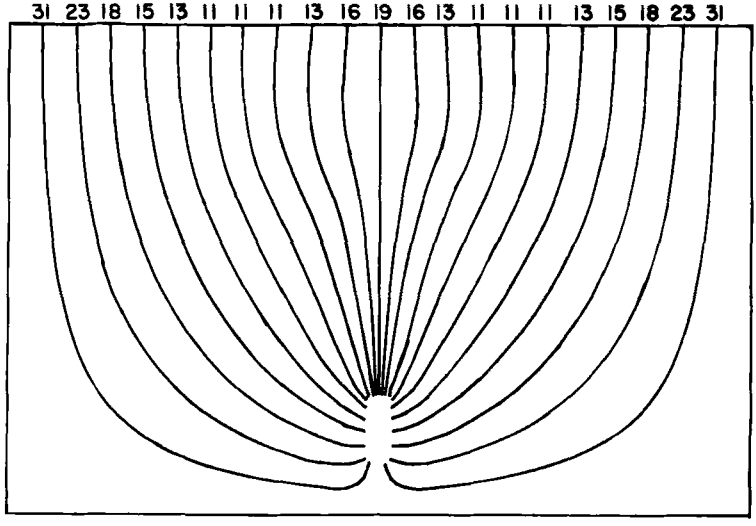

FIG. 14. Streamlines in the presence of a low permeability lens in the upper central portion of the domain. See Fig. 13 and Tables 2 and 3 for parameter values. Run 10.

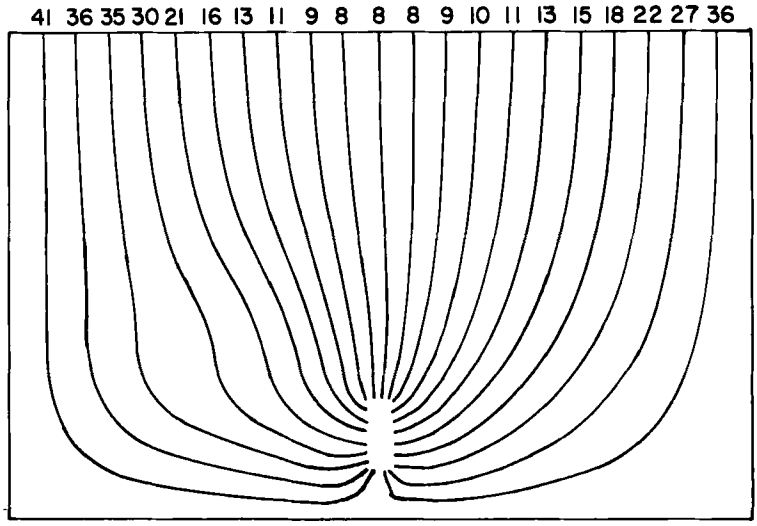

FIG. 15. Streamlines in the presence of a low permeability lens in the lower left portion of the domain. See Fig. 13 and Tables 2 and 3 for parameter values. Run 14.

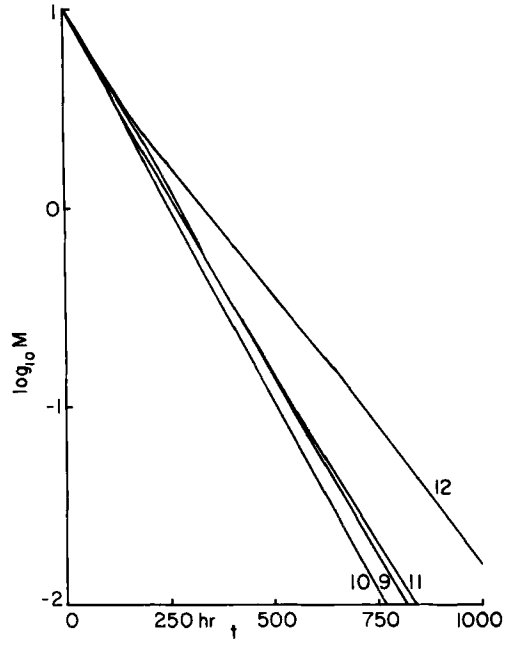

FIG. 16. Plots of $\log_{10}(M_{\text{total}})$ versus t for Runs 9–12, as indicated by the numbers by the plots. See Fig. 13 and Tables 2 and 3 for parameter values.

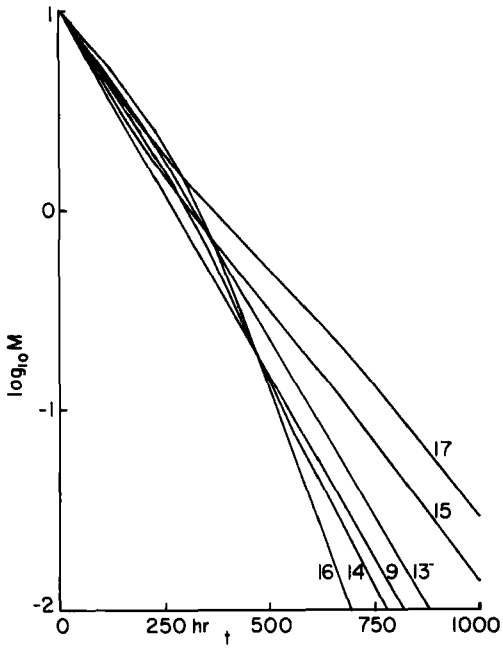

FIG. 17. Plots of $\log_{10}(M_{total})$ versus t for Runs 9 and 13–16 as indicated by the numbers by the plots. See Fig. 13 and Tables 2 and 3 for parameter values.

into the lower left corner of the domain, increasing the rate of cleanup. In Run 16 (Fig. 17), lenses on both sides of the domain divert the flow of soil gas toward the lower left and right corners, resulting in a quite significant improvement in removal rate. The two runs showing the greatest increase in 99% cleanup time are Runs 12 and 15, in which the lenses are very near the edge of the domain.

These results (for Runs 9–17) are rather similar to the results obtained in Runs 1–8 with somewhat different geometry. If one knows the location(s) of any low-permeability regions in the domain to be vapor stripped, this approach could be used to optimize the siting of the wells.

In Run 17 the low permeability lens is located directly beneath the well. As seen in Table 4, although the 50% cleanup time of this run is comparable to those of the other runs, its 99% cleanup time is far longer than the 99% cleanup times of Runs 9–16, and is double that of the reference run, 9, which has no lenses. Run 17 illustrates the point that a rapid initial rate of contaminant removal does not guarantee near-optimal efficiency of removal along toward the end of the vapor-stripping process. The converse may also be true; Run 13 has the largest 50% cleanup time of these nine runs, yet its 99% cleanup time is less than those of Runs 12, 15, and 17.

TABLE 4
Results Obtained with Systems Containing Low Permeability Lenses (Runs 9–17); Parameters Given in Tables 2 and 3

Run	x_i (m)	y_i (m)	t(90%) (h)	t(99%) (h)	Gas flux (mmol/s)
9	—	—	271	545	718.1
10	12.50	10.00	250	509	628.0
11	6.25	10.00	280	551	650.6
12	1.00	10.00	333	714	691.1
13	12.50	4.00	315	595	457.7
14	6.25	4.00	304	533	612.5
15	1.00	4.00	310	688	695.0
16	6.25	4.00	327	512	297.3
	18.75	4.00			
17	12.50	0.00	366	795	362.8

The runs shown here indicate the feasibility of taking into account inhomogeneities in the permeability when modeling soil vapor stripping, provided that the necessary data base is available. The runs also indicate that the damaging effects of such low permeability regions can usually be reduced to an acceptable level by proper placement and design of the well system. Low permeability lenses centered near the border separating two adjacent zones of influence are likely to be damaging. The screening of a well within or over a region of low permeability greatly reduces the rate of cleanup and should be avoided if at all possible. The other configurations studied yielded cleanup rates only slightly different from the cleanup rate found for a homogeneous domain of influence.

EFFECTS OF SOIL MOISTURE; ANALYSIS

A potentially major factor affecting the pneumatic permeability is the soil moisture content. A formula proposed by Millington and Quirk (*15*) for the relationship between pneumatic permeability and volumetric moisture content has been fairly widely used; it can be written as

$$K(w) = K_0 \left(\frac{u - w}{u}\right)^{10/3} = K_0(1 - R_h)^{10/3} \tag{35}$$

where K_0 = (pneumatic) permeability of dry soil
u = total voids fraction
w = volumetric water content
$R_h = w/u$

A plot of $K(w)/K_0$ versus R_h is shown in Fig. 18; a significant moisture content results in a very marked decrease in the permeability.

Generally the underlying boundary to a domain being vapor stripped is the water table, at a depth b below the surface of the soil. We therefore consider a model in which R_h varies from 1 (saturation) at the water table to a value R_{ha} at the surface of the soil, where R_{ha} is determined by the atmospheric relative humidity and the recent history of rainfall events. We assume that R_h is given by the following function, which satisfies these limiting conditions:

$$R_h(y) = 1 - (1 - R_{ha})(y/b)^{\alpha} \tag{36}$$

where y = distance above the water table
α = adjustable parameter; $0 < \alpha < \infty$

Then the equation

$$K(y) = K_0[(1 - R_{ha})(y/b)^{\alpha}]^{10/3} \tag{37}$$

can be used to calculate K_x and K_y, the horizontal and vertical components of the permeability tensor, by substituting $K_0 = K_{0x}$ or K_{0y}. Plots of y/b versus R_h for various values of α are given in Fig. 19.

The volumetric water content $w(y)$ is given by

$$w(y) = uR_h = u[1 - (1 - R_{ha})(y/b)^{\alpha}] \tag{38}$$

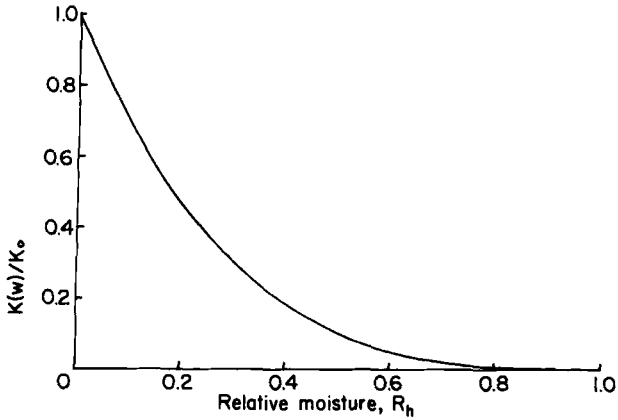

FIG. 18. Plot of $K(w)/K_0$ versus relative moisture content R_h according to Eq. (35).

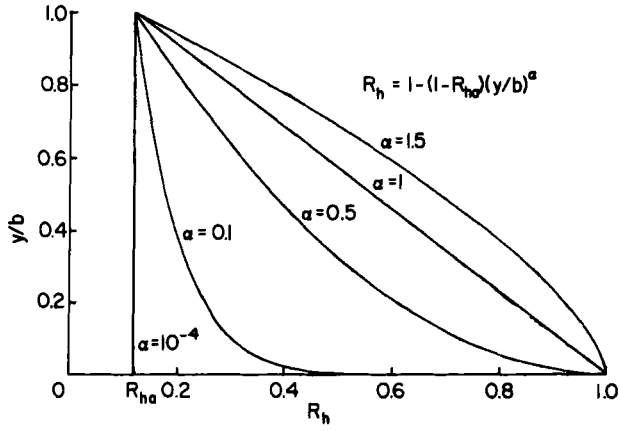

FIG. 19. Plot of y/b versus relative moisture content R_h. y = height above the water table, b = distance between the water table and the surface of the soil. R_{ha} = 0.12. See Eq. (36).

and the air-filled voids fraction is

$$v(y) = u - w(y) \tag{39}$$

The soil gas velocity field in the domain of interest is then calculated, as before, by the overrelaxation method. The removal of contaminant is described by

$$\partial m/\partial t = -\nabla \cdot \mathbf{v}c_v \tag{40}$$

where m = mass of contaminant per unit volume of soil
$\mathbf{v}$ = soil gas velocity
c_v = vapor concentration of contaminant

Now we assume

$$c_v = K_H c_l \tag{41}$$

where

c_l = contaminant concentration in the soil moisture

Also

$$m = vc_v + wc_l \tag{42}$$

from which we obtain, after substitution and rearrangement,

$$c_v = \frac{m}{v + w/K_H} = \frac{m}{u + w(K_H^{-1} - 1)} \tag{43}$$

Substitution of this result in Eq. (40) then yields

$$\frac{\partial m}{\partial t} = -\nabla \cdot \left(\frac{vm}{u + w(y)(K_H^{-1} - 1)} \right) \tag{44}$$

Note that this equation differs from Eq. (30) in that w in Eq. (30) was assumed independent of position, which permits one to put the denominator to the left of the divergence operator.

Equation (44) can then be solved numerically by the same procedure used to solve Eq. (30).

SOIL MOISTURE; RESULTS

A set of five runs (18–22) was made using the model parameter values given in Table 2 and the values of α, the moisture distribution parameter defined in Eq. (36), of 10^{-4}, 0.1, 0.5, 1, and 1.5; these were the values used in making the plots of depth versus R_h shown in Fig. 19. Figures 20

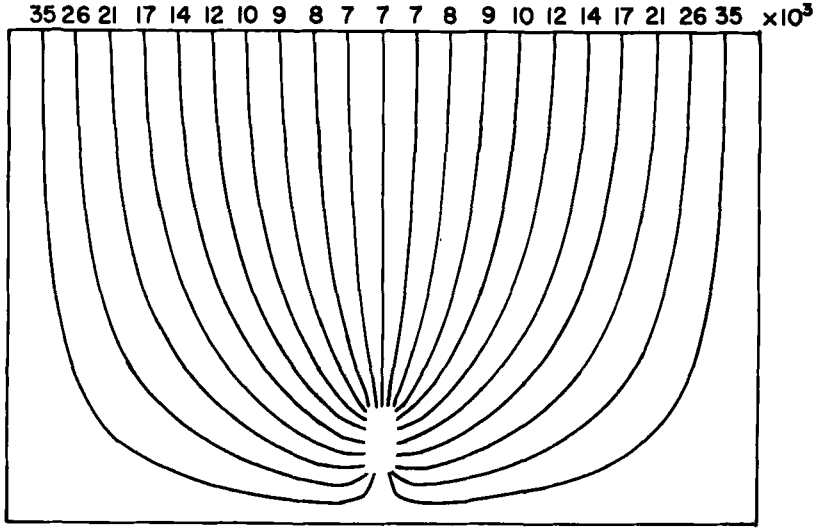

FIG. 20. Streamlines in a homogeneously rather dry soil ($\alpha = 10^{-4}$). See Fig. 19. Other parameters as in Table 2.

and 21 show the streamlines obtained for $\alpha = 10^{-4}$ (dry soil, $R = 0.12$ throughout and 1.0 (linear distribution of moisture with depth from saturation at the water table to a value of R_h of 0.12 at the surface). Two main differences between these figures are seen. First, at the higher moisture content (Fig. 21) there are large increases in the transit times required for soil gas to move along the streamlines from the soil surface to the well. Near the well axis the increase is by a factor of about 40. Near the edge of the domain the increase in transit time is by a factor of about 160.

Second, comparison of the streamlines in Figs. 20 and 21 shows that at the higher moisture content (Fig. 21) the streamlines have a very marked tendency to shortcut their way to the well, avoiding the lower corners of the domain. Cleanup of these regions is therefore expected to be extremely slow.

Thus we see from examination of the streamlines and transit times alone that one may expect a drastic decrease in soil vapor stripping efficiency if the soil being stripped has a moisture content that is near saturation over an appreciable volume of the lower part of the domain of interest.

The results of modeling vapor stripping by means of Eq. (44) are summarized in Table 5 and Figs. 22 and 23. Runs 18–22, which correspond to

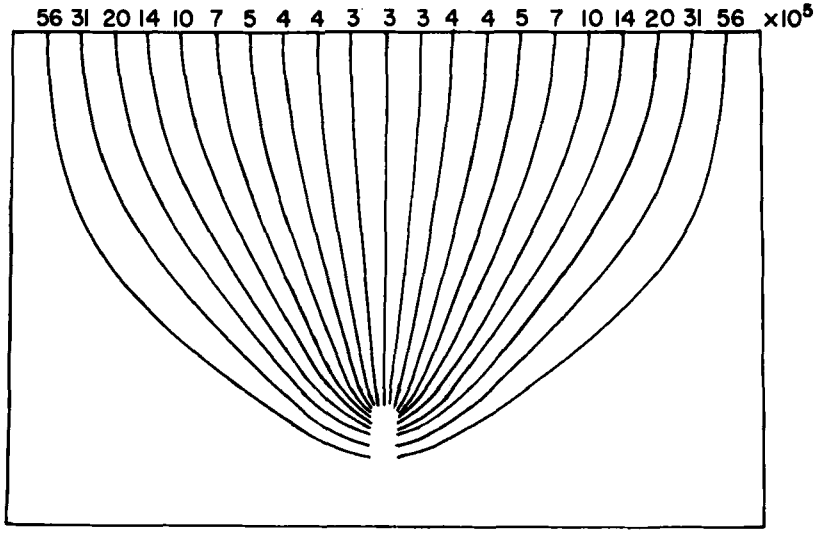

FIG. 21. Streamlines in a soil which becomes progressively more wet with increasing depth ($\alpha = 1$). See Fig. 19. Other parameters as in Table 2.

TABLE 5
Effects of Varying Soil Moisture, Runs 18–38. Parameters as in Table 2 Except as Indicated

Run	Modified parameter(s)	Moisture parameter α	t(50%) (s)	t(99%) (s)	Total soil gas flux (mmol/s)
18	—	10^{-4}	2.88 E5	1.97 E6	747.7
19	—	0.1	6.07 E5	1.34 E7	502.3
20	—	0.5	1.18 E7	5.46 E9	93.40
21	—	1.0	2.88 E8	8.82 E12	10.20
22	—	1.5	5.88 E9	1.68 E16	1.05
23	Height of bottom of well above water table = 0.6 m Height of top of screened section of well above water table = 2.4 m	10^{-4}	3.07 E5	2.01 E6	674.3
24	Height of bottom of well above water table = 0.6 m Height of top of screened section of well above water table = 2.4 m	1.0	5.22 E8	1.68 E13	4.67
25	Height of bottom of well above water table = 1.2 m Height of top of screened section of well above water table = 1.8 m	10^{-4}	3.73 E5	2.40 E6	567.1
26	Height of bottom of well above water table = 1.2 m Height of top of screened section of well above water table = 1.8 m	1.0	1.26 E9	4.11 E13	1.77
27	Overlying impermeable cap of width 12 m	10^{-4}	3.16 E5	1.83 E6	644.4
28	Overlying impermeable cap of width 12 m	1.0	2.45 E8	7.61 E12	10.31
29	K_{v0} = 0.05 m²/atm · s	10^{-4}	4.33 E5	2.40 E6	474.0
30	K_{v0} = 0.05 m²/atm · s	1.0	2.32 E8	3.71 E12	6.75
31	K_{v0} = 0.20 m²/atm · s	10^{-4}	2.15 E5	1.93 E6	1082.4
32	K_{v0} = 0.20 m²/atm · s	1.0	4.58 E8	2.52 E13	15.92

(*continued*)

TABLE 5 (*continued*)

Run	Modified parameter(s)	Moisture parameter α	t(50%) (s)	t(99%) (s)	Total soil gas flux (mmol/s)
33	K_{x0} = 0.05 m²/atm · s	10^{-4}	4.33 E5	3.86 E6	563.8
34	K_{x0} = 0.05 m²/atm · s	1.0	9.21 E8	5.11 E13	7.96
35	K_{x0} = 0.20 m²/atm · s	10^{-4}	2.16 E5	1.20 E6	948.0
36	K_{x0} = 0.20 m²/atm · s	1.0	7.52 E8	1.85 E12	13.49
37	Domain width = 12.5 m, initial contaminant mass = 5 kg	10^{-4}	1.94 E5	9.42 E5	548.9
38	Domain width = 12.5 m, initial contaminant mass = 5 kg	1.0	6.31 E8	5.24 E12	8.82

progressively larger values of α (10^{-4}, 0.1, 0.5, 1, 1.5) and wetter soils, exhibit extremely large increases of both 50 and 99% cleanup times. In Runs 23–38, changes are made in various parameters in the model, and calculations are made with dry soil ($\alpha = 10^{-4}$, $R_h = 0.12$) and wet soil ($\alpha = 1$). In every case we see a massive increase in 50 and 99% cleanup times with increasing soil moisture.

Let us examine these runs in more detail. We consider first the runs involving rather dry soil, for which $\alpha = 10^{-4}$. Comparison of Runs 18 and 23 indicates that moving the screened section of the well lower (by 0.6 m) has relatively little effect on either t(50%) or t(99%). Comparison of Runs 18 and 25 shows a decrease in the flow rate of the soil gas with decreasing length of the screened section of the well (from 1.8 to 0.6 m); associated with this we find moderate increases in both t(50%) and t(99%), as one would expect. The effect of an overlying impermeable cap is seen on comparing Runs 18 and 27; there is some reduction in flow rate, a slight increase in t(50%), and a slight decrease in t(99%). Increasing the permeabilities K_x or K_y increases gas flow rate and rates of cleanup; this is particularly noticeable for increases in K_x. Compare Run 18 with Runs 29, 31, 33, and 35. Decreasing the width of the domain from 25 m to 12.5 m roughly doubles the rate of cleanup, as seen by comparing Run 18 with Run 37.

At high moisture content ($\alpha = 1.0$) the effects of varying the model parameters are generally qualitatively similar to what we have seen above,

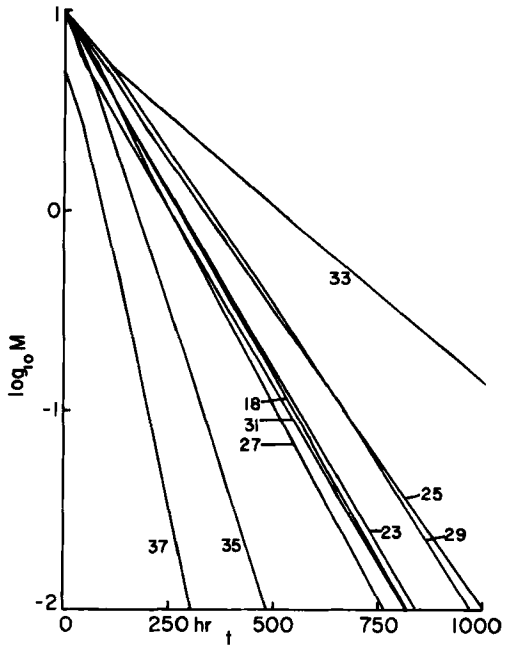

FIG. 22. Plots of $\log_{10}(M_{total})$ versus time (h) for runs simulating rather dry soils ($\alpha = 10^{-4}$). See Table 5 for gas flow rates, times for 50 and 99% clean up. Model parameters are given in Tables 2 and 5.

but tend to be larger in magnitude. Moving the screened section of the well to lower depths (where the permeability is much smaller) roughly doubles both $t(50\%)$ and $t(99\%)$, as seen in Runs 21 and 24. Comparison of Runs 21 and 26 shows that decreasing the length of the screened section of the well decreases the soil gas flow rate to about 28% of its original value, resulting in increases in cleanup times by factors of over 4. The presence of an overlying impermeable cap results in modest decreases in both $t(50\%)$ and $t(99\%)$ here, in contrast to the result found with $\alpha = 10^{-4}$. Effects of changes in the permeabilities and in the width of the domain are fairly similar to those which were observed with $\alpha = 10^{-4}$.

We conclude that the vapor stripping of rather wet soils is likely to be a very slow process. In such situations, efforts to reduce surface recharge, to draw down the level of the water table by pumping, and to allow adequate time for soil drainage after the water table has been drawn down

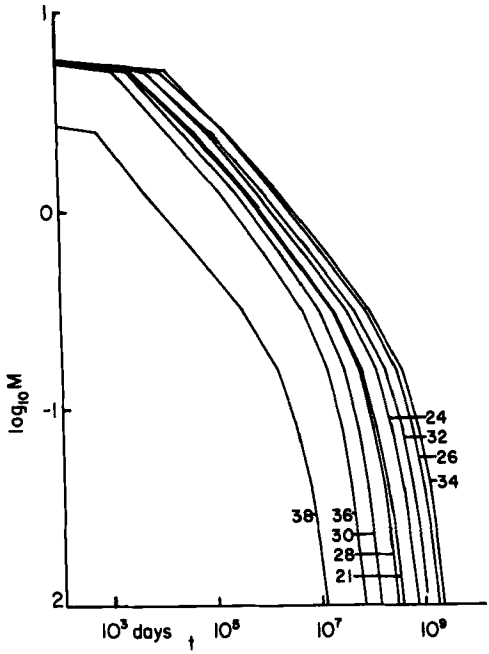

FIG. 23. Plots of $\log_{10}$ (M_{total}) versus time (days) for runs simulating quite wet soils. The time scale in this figure is logarithmic. See Table 5 for gas flow rates, times for 50 and 99% cleanup. Model parameters are given in Tables 2 and 5.

may be necessary in order to achieve acceptable contaminant removal rates by soil vapor stripping.

Acknowledgments

We are indebted to Eckenfelder, Inc., and the Water Resources Research Center of the University of Tennessee for support of this work. C.G.-L. is obliged to the Spanish Government for a grant.

REFERENCES

1. R. E. Osejo and D. J. Wilson, *Sept. Sci. Technol.*, Submitted.
2. D. J. Wilson, A. N. Clarke, and J. H. Clarke, *Ibid., 23,* 991 (1988).
3. O. K. Gannon, D. J. Wilson, A. N. Clarke, R. D. Mutch Jr., and J. H. Clarke, *Ibid., 24,* 831 (1989).
4. D. J. Wilson, A. N. Clarke, and R. D. Mutch Jr., *Ibid., 24,* 939 (1989).
5. R. D. Mutch Jr. and D. J. Wilson, *Ibid., 25,* 1 (1990).
6. D. J. Wilson, *Ibid., 25,* 243 (1990).

7. G. E. Hoag, A. L. Baehr, and M. C. Marley, "In-Situ Recovery of Hydrocarbon Contaminated Soil Utilizing the Induced Soil Venting Process," in *Management of Hazardous Toxic Wastes in the Process Industry [International Congress]*, (S. T. Kolaczkowski and B. D. Crittenden, eds.), Elsevier, London, 1987, p. 273.
8. A. L. Baehr, G. E. Hoag, and M. C. Marley, *J. Contam. Hydrol., 4,* 1 (1989).
9. N. J. Hutzler, D. B. McKenzie, and J. S. Gierke, "Vapor Extraction of Volatile Organic Chemicals from Unsaturated Soil," in *Abstracts, International Symposium on Processes Governing the Movement and Fate of Contaminants in the Subsurface Environment,* Stanford, California, July 23–26, 1989.
10. W. A. Jury, in *Vadose Zone Modeling of Organic Pollutants* (S. C. Hern and S. M. Melancon, eds.), Lewis Publishers, Chelsea, Michigan, 1986, Chap. 11.
11. R. A. Freeze, *Water Resour. Res., 11,* 725 (1975).
12. Oak Ridge National Laboratory, Draft: *Preliminary Test Plan, in-situ Soil Venting Demonstration, Hill AFB, Utah,* U.S. Air Force Engineering and Services Center, Tyndall AFB, Florida, 1987.
13. Rollins, Brown, and Gunnell, Inc., *Subsurface Investigation and Remedial Action, Hill AFB JP-4 Fuel Spill, Provo, Utah,* U.S. Air Force, Hill AFB, Utah, 1985.
14. R. A. Freeze and J. A. Cherry, *Groundwater,* Prentice-Hall, Englewood Cliffs, New Jersey, 1979, p. 184.
15. R. J. Millington and J. M. Quirk, *Trans. Faraday Soc., 57,* 1200 (1961).

Received by editor March 6, 1990